GMR
The Original

IN SILICO PRIORITIZATION OF *GLYCINE MAX* PHYTOCOMPOUNDS AGAINST PCOS-ASSOCIATED TARGETS AND PHYSICOCHEMICAL CHARACTERIZATION OF ZIRCONIA NANOPARTICLES

Ayesha Zubair[1]*, Asma Ahmad[2], Shazia Shaheen[3], Khurram Munir[4], Fahad Sarfraz[5]
[1,2]Institute of Molecular Biology and Biotechnology, The University of Lahore, Lahore, Pakistan.
[3]Department of Gynaecology and Obstetrics, Allied Hospital-I, Faisalabad Medical University, Faisalabad, Pakistan
[4]Assistant Professor, Department of Physiology, Sheikh Zayed Medical College, Rahim Yar Khan, Pakistan
[5]Associate Professor, CMH Lahore Medical College & Institute of Dentistry, Lahore, Pakistan
***Corresponding author:** Ayesha Zubair, Email: drayeshazubair@gmail.com

ABSTRACT
Polycystic ovary syndrome (PCOS) is a heterogeneous endocrine-metabolic disorder in which multi-target molecular dysregulation and limitations of conventional drug delivery support investigation of integrated computational and nanomaterial strategies. This study combined In Silico screening of a finalized 30-ligand *Glycine max* (L.) Merr. seed phytocompound dataset with physicochemical characterization of zirconia nanoparticles (ZrO_2 NPs). Thirty GC-MS-guided ligands were screened against ten selected proteins involved in apoptosis, cellular stress, redox regulation, nutrient sensing and metabolic signaling. The strongest predicted ligand-protein interactions in the top-ranked dataset ranged from -8.0 to -8.9 kcal/mol. Carbonic acid, 2-dimethylaminoethyl isobutyl ester (CADIE) was prioritized for focused analysis because it appeared as the lead compound in the MAGE-A3 output, binding in pocket C1 at -8.00 kcal/mol and interacting with ASN94, ALA95, THR98, TYR101, VAL104, ASP105, CYS144, VAL148, PHE149, MET183 and TYR224. CADIE showed a molecular weight of 189.25 g/mol, TPSA of 38.77 Å^2, seven rotatable bonds, four hydrogen-bond acceptors, no Lipinski violation, high predicted gastrointestinal absorption and no predicted P-glycoprotein substrate liability. Molecular-dynamics analysis reported a mean RMSD of 1.4 Å and a maximum of 1.9 Å over 100 ns. ZrO_2 synthesis produced a creamy-white material; UV-visible analysis showed an absorption maximum near 378 nm, XRD showed a crystalline diffraction pattern, and SEM indicated irregular/rough nanoscale particles with an average size of approximately 62 nm. Dispersion analysis, however, revealed a near-neutral zeta potential (+0.91 mV) and a volume-weighted mean particle size of 12.0934 µm, corresponding to an aggregate-to-primary-size ratio of approximately 195. These findings support computational prioritization of CADIE and successful formation of nanoscale zirconia, while also demonstrating that colloidal stabilization is required before the carrier can be considered formulation-ready.

KEYWORDS: *Glycine max*; polycystic ovary syndrome; molecular docking; MAGE-A3; CADIE; zirconia nanoparticles; XRD; SEM; zeta potential.

1. INTRODUCTION

Polycystic ovary syndrome (PCOS) is a complex reproductive-endocrine and metabolic disorder characterized by ovulatory dysfunction, hyperandrogenism and polycystic ovarian morphology, with frequent coexistence of insulin resistance, oxidative stress, inflammatory signaling and altered follicular survival [1-5]. The biological heterogeneity of PCOS makes single-target therapeutic interpretation difficult and encourages strategies that can evaluate several molecular pathways in parallel [1,2].

Plant-derived phytocompounds provide chemically diverse scaffolds that may interact with multiple signaling proteins. *Glycine max* (L.) Merr. seeds contain fatty-acid derivatives, sterols, tocopherols and other small molecules with potential endocrine, metabolic and antioxidant relevance. Computational screening is useful for organizing such chemically diverse datasets because molecular docking can prioritize ligand-protein combinations for subsequent experimental validation [10,11]. Importantly, docking scores represent predicted affinity rather than biological efficacy and should be interpreted together with structural quality, drug-likeness and molecular-dynamics behavior.

Nanotechnology provides a complementary strategy for improving delivery of bioactive compounds. Nanomaterial-based systems have been explored in PCOS models to enhance stability, modulate exposure and combine therapeutic functions [6-9]. Zirconium dioxide (zirconia; ZrO_2) is a chemically robust ceramic material that can be synthesized in nanoscale form, including through plant-assisted approaches [12]. For biomedical development, however, nanoparticle identity and morphology are not sufficient: crystallinity, particle size, aggregation and surface charge

must be considered because these variables influence dispersion, reproducibility and downstream loading behavior [13-15].

The present study therefore integrates two complementary components of a larger PCOS research program: (i) In Silico screening of 30 Glycine max-derived ligands against a ten-protein target panel, including focused assessment of carbonic acid, 2-dimethylaminoethyl isobutyl ester (CADIE) with MAGE-A3; and (ii) physicochemical characterization of synthesized zirconia nanoparticles. In addition to the analyses reported in the dataset, a secondary size-integration analysis was performed to quantify the magnitude of particle aggregation by comparing SEM primary-particle size with suspension-based particle-size distribution.

2. MATERIALS AND METHODS

2.1. Study design, duration and ligand dataset

This experimental study was conducted from October 2025 to January 2026 at the Institute of Molecular Biology and Biotechnology (IMBB), The University of Lahore, Lahore, Pakistan, in collaboration with the relevant analytical facilities. The present investigation comprised two interconnected phases: *In Silico* screening and molecular interaction analysis of selected *Glycine max* (L.) Merr. phytocompounds against selected protein targets, followed by the synthesis and physicochemical characterization of zirconia nanoparticles (ZrO_2 NPs).The study was designed as a combined phytochemical-computational and nanomaterial-characterization investigation. Polarity-based *Glycine max* (L.) Merr. seed extracts were previously analyzed by GC-MS, and 30 compounds were retained as the finalized ligand dataset. Relative chromatographic abundance was used only to describe the analytical profile and not as a surrogate for biological potency. The selected ligands were advanced to molecular screening against a ten-protein panel.

2.2. Protein target panel

The final docking panel comprised induced myeloid leukemia cell differentiation protein (MCL1), constitutive coactivator of PPAR-gamma-like protein 1 (FAM120A), thioredoxin-related transmembrane protein 2 (TMX2), melanoma-associated antigen 3 (MAGE-A3), nicastrin (NCSTN), cell-cycle progression protein 1 (CCPG1), legumain (LGMN), sodium-coupled neutral amino-acid transporter 2 (SLC38A2), heat-shock protein 70 (HSP70), and BCL-2-like protein 11 (BIM). These proteins were selected to represent cellular processes related to apoptosis, oxidative-stress response, ER-mitochondrial communication, protein turnover, antigen processing, nutrient sensing, metabolism and molecular chaperoning. Three-dimensional receptor structures were obtained from UniProt/structure-model resources and prepared by removal of water molecules and energy minimization before docking.

Table 1. Final ten-protein panel used for molecular docking and the biological functions used to frame interpretation.

Protein	Functional context
MCL1	Anti-apoptotic survival regulator
FAM120A	PPAR-gamma-related coactivation, mRNA stability and lipid-gene regulation
TMX2	ER-mitochondrial contact, calcium flux and redox balance
MAGE-A3	Selected regulatory protein used for focused lead-compound analysis
NCSTN	Gamma-secretase structural subunit
CCPG1	ER-phagy/protein-quality control
LGMN	Protease involved in antigen processing and matrix remodeling
SLC38A2	Neutral amino-acid transport and nutrient sensing
HSP70	Stress-response molecular chaperone
BIM	Pro-apoptotic BH3-only protein

2.3. Ligand preparation, docking and interaction analysis

Ligand structures were obtained in structure-data-file format and converted to docking-compatible formats. Docking was performed using a PyRx/AutoDock Vina-based workflow, with predicted binding pockets evaluated before pose selection. Protein-ligand complexes were examined in Discovery Studio and related interaction-visualization tools to identify binding residues. Binding energies are reported in kcal/mol, with more negative values interpreted as stronger predicted binding. Comparable GC-MS-guided docking approaches have been applied to PCOS-related target screening [10].

2.4. Physicochemical, pharmacokinetic and drug-likeness screening

The 30 ligands were assessed using computational physicochemical and ADME descriptors, including molecular weight, hydrogen-bonding capacity, topological polar surface area (TPSA), rotatable bonds, lipophilicity-related parameters, gastrointestinal absorption, P-glycoprotein substrate status and standard drug-likeness filters. CADIE was subsequently examined in greater detail because of its position in the MAGE-A3 docking output. Where individual CYP predictions were recorded as temporarily unavailable in the dataset, no metabolic-enzyme conclusion was drawn in the present manuscript.

2.5. Molecular-dynamics analysis

The CADIE-MAGE-A3 complex was evaluated by molecular-dynamics simulation over 100 ns. Structural stability was assessed using root-mean-square deviation (RMSD) and residue flexibility by root-mean-square fluctuation (RMSF). Trajectory interpretation focused on maintenance of the ligand-binding configuration and changes in active-site residue behavior. Molecular-dynamics findings were treated as computational stability evidence rather than direct target-engagement proof.

2.6. Zirconia nanoparticle synthesis

Zirconium chloride was used as the precursor. A nominal 0.1 M precursor solution was prepared by dissolving approximately 1.36 g of zirconium chloride in 100 mL double-distilled water under magnetic stirring. Plant-derived extract was introduced gradually as a reducing/stabilizing medium, and the pH was adjusted with alkaline solution to support hydrolysis and precipitation. Formation of a creamy-white precipitate was used as the initial visual indicator of nanoparticle formation. The material was separated by centrifugation, repeatedly washed with double-distilled water and ethanol, dried, and calcined where required to improve crystallinity. Plant-assisted routes have previously been reported for zirconia nanoparticle production [12].

2.7. Zirconia nanoparticle characterization

The dataset included UV-visible spectroscopy, FTIR, X-ray diffraction (XRD), scanning electron microscopy (SEM), and zeta-potential/particle-size distribution measurements. The present article emphasizes UV-visible/FTIR summary data, XRD crystallinity, SEM morphology and zeta/particle-size distribution because these datasets provide directly interpretable optical, structural, morphological and colloidal information for the synthesized zirconia preparation.

2.8. Secondary integrative size analysis

A secondary aggregation analysis was calculated from the reported characterization data. The volume-weighted mean suspension diameter (12.0934 μm) and median diameter (D50 = 8.7672 μm) were converted to nanometers and divided by the reported SEM mean particle size (62 nm). This yielded a mean aggregate-to-primary-size ratio of approximately 195.1 and a D50-to-primary-size ratio of approximately 141.4. This calculation did not generate new experimental data; it integrates existing dry-state and suspension-state measurements to quantify aggregation behavior.

3. RESULTS

3.1. Multi-target molecular docking profile

The docking dataset showed favorable predicted interactions across the selected protein panel. Among the strongest reported ligand-protein combinations, binding energies ranged from -8.0 to -8.9 kcal/mol. Cannabinol, pentafluoropropionate and gamma-tocopherol appeared repeatedly among high-ranking interactions, supporting a multi-target pattern rather than a single-protein signal. The most negative reported scores reached -8.9 kcal/mol in pocket C4 for several ligand-protein combinations. These results should be interpreted as prioritization signals because docking does not directly measure biological efficacy.

Table 2. Representative strongest predicted ligand-protein interactions reported in the finalized docking dataset.

Protein	Ligand	Pocket	Binding energy (kcal/mol)
HSP70	Cannabinol, pentafluoropropionate	C1	-8.10
MCL1	Campesterol	C1	-8.60
BIM	Gamma-tocopherol	C1	-8.10
CCPG1	Gamma-tocopherol	C1	-8.10
FAM120A	Gamma-tocopherol	C1	-8.10
MAGE-A3	CADIE	C1	-8.00
TMX2	Cannabinol, pentafluoropropionate	C1	-8.10
MCL1	Cannabinol, pentafluoropropionate	C4	-8.90
FAM120A	Cannabinol, pentafluoropropionate	C4	-8.90
NCSTN	Docosanoic acid, ethyl ester	C4	-8.90
NCSTN	Campesterol	C4	-8.90
CCPG1	Benzenepropanoic acid derivative	C4	-8.80
LGMN	Methyl 7,12-octadecadienoate	C4	-8.80

3.2. CADIE interaction with MAGE-A3 and lead descriptors

Within the MAGE-A3 output, CADIE appeared as the focused lead compound in pocket C1 with a predicted binding energy of -8.00 kcal/mol. The reported interaction network included ASN94, ALA95, THR98, TYR101, VAL104, ASP105, CYS144, VAL148, PHE149, MET183 and TYR224. The MAGE-A3 structural model showed 83.6% of non-glycine/non-proline residues in the most favored Ramachandran regions and 94.9% in favored plus additionally

allowed regions; 2.5% of residues were reported in disallowed regions. This supports a usable but non-ideal model and warrants caution in mechanistic interpretation.

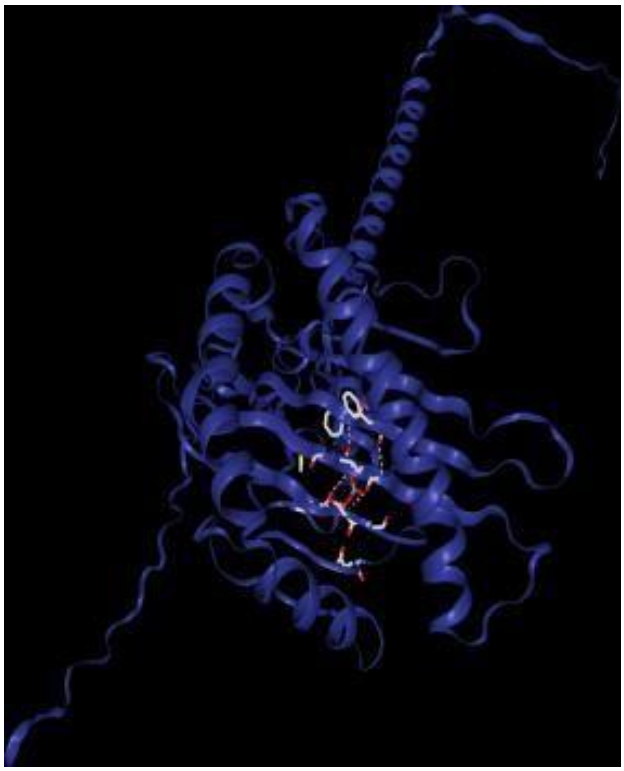

Fig. 1. Representative docked corresponding to the CADIE-MAGE-A3 analysis.

Table 3. Physicochemical, pharmacokinetic and drug-likeness descriptors reported for CADIE.

Descriptor	Reported value
Molecular formula	C9H19NO2
Molecular weight	189.25 g/mol
Heavy atoms	13
Fraction Csp3	0.89
Rotatable bonds	7
H-bond acceptors/donors	4 / 0
Molar refractivity	51.03
TPSA	38.77 Å²
GI absorption	High
P-gp substrate	No
Log Kp	-6.11 cm/s
Lipinski	Yes; 0 violations
Ghose / Veber / Egan	Pass / Pass / Pass
Muegge	No; MW < 200
Bioavailability score	0.55

3.3. Molecular-dynamics stability of the CADIE-MAGE-A3 complex

The CADIE-MAGE-A3 complex showed an overall mean RMSD of 1.4 Å and a reported maximum of 1.9 Å over the simulation period. Methionine residues MET74, MET77, MET119 and MET277 were reported among interacting residues, together with GLY40, GLN43 and PHE96. The trajectory analysis described localized secondary-structure changes in fluctuating regions while maintaining overall complex stability. These observations provide computational support for persistence of the docked complex but do not establish a validated PCOS mechanism.

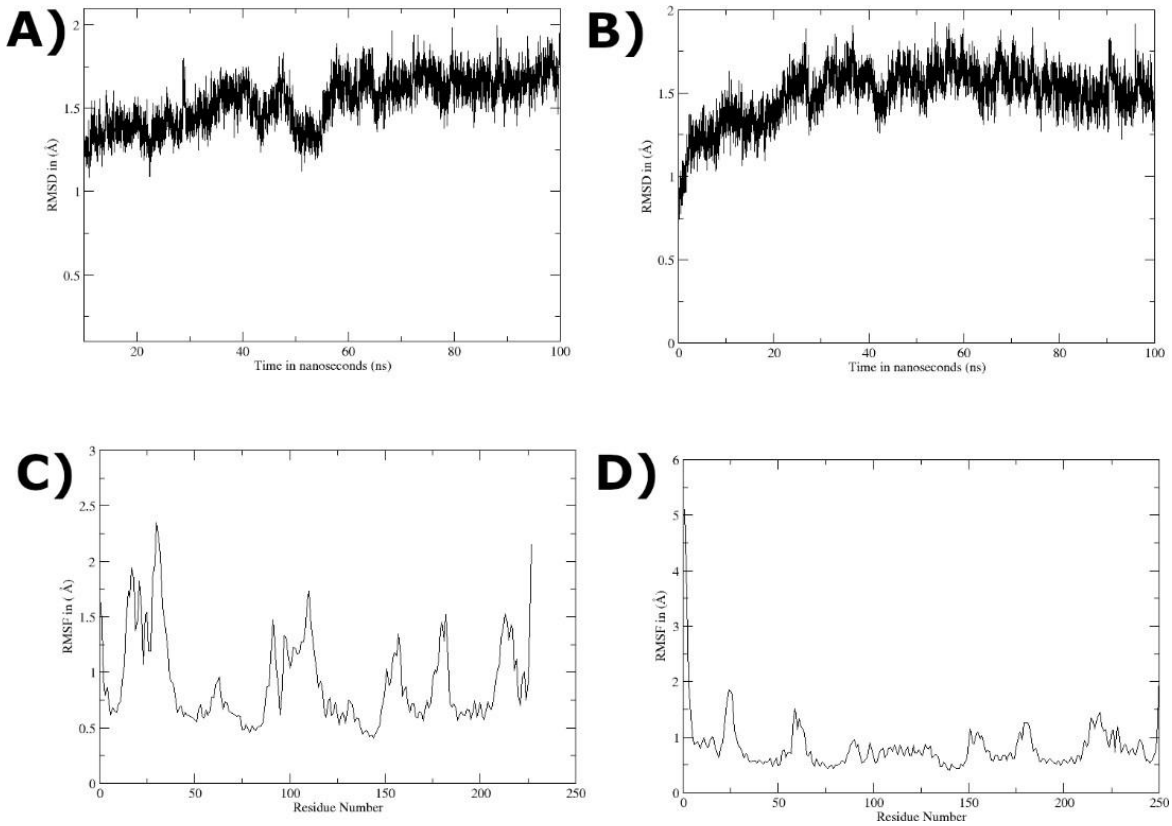

Fig. 2. Molecular-dynamics plots reported for the selected ligand-protein complex, including RMSD- and RMSF-based stability/flexibility profiles over the 100-ns trajectory.

3.4. Zirconia nanoparticle formation and structural characterization

Nanoparticle formation was initially indicated by development of a creamy-white/whitish precipitate or powder. UV-visible analysis showed a characteristic absorption peak near 378 nm, with a reported optical band-gap estimate of approximately 3.6 eV. FTIR peaks were reported at 3425.15 and 1433.07 cm^{-1} (assigned to O-H-related vibrations), 2920.85 cm^{-1} (C-H), 1629.07 cm^{-1} (C=C) and 1112.53 cm^{-1} (C=O-related assignment), supporting the presence of surface-associated functional groups.

XRD analysis demonstrated a crystalline diffraction pattern with principal reflections reported around 25°, 30°, 35°, 40°, 45°, 50° and 60° 2θ. The pattern was interpreted using JCPDS card no. 03-065-2880. The diffractogram therefore supports formation of a crystalline inorganic phase in the synthesized material.

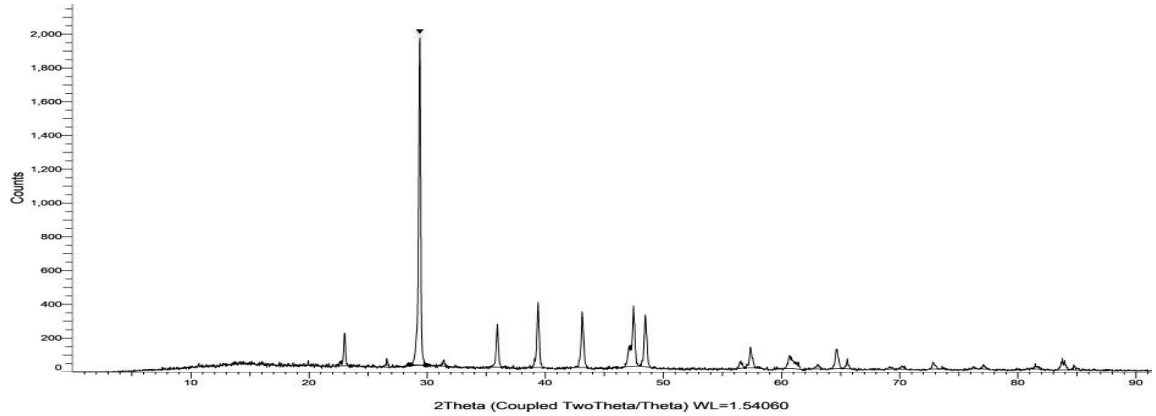

Fig. 3. X-ray diffraction pattern of the synthesized zirconia nanoparticle preparation showing the reported crystalline diffraction profile.

3.5. SEM morphology

SEM micrographs showed nanoscale particle domains with predominantly rough/irregular morphology, a tendency toward polygonal/hexagonal outlines in some fields, and visible agglomeration. The reported average particle size was approximately 62 nm. The wide range of magnifications demonstrated that nanoscale primary particles coexisted with

larger clustered structures, indicating that dry-state morphology and suspension behavior should be interpreted together.

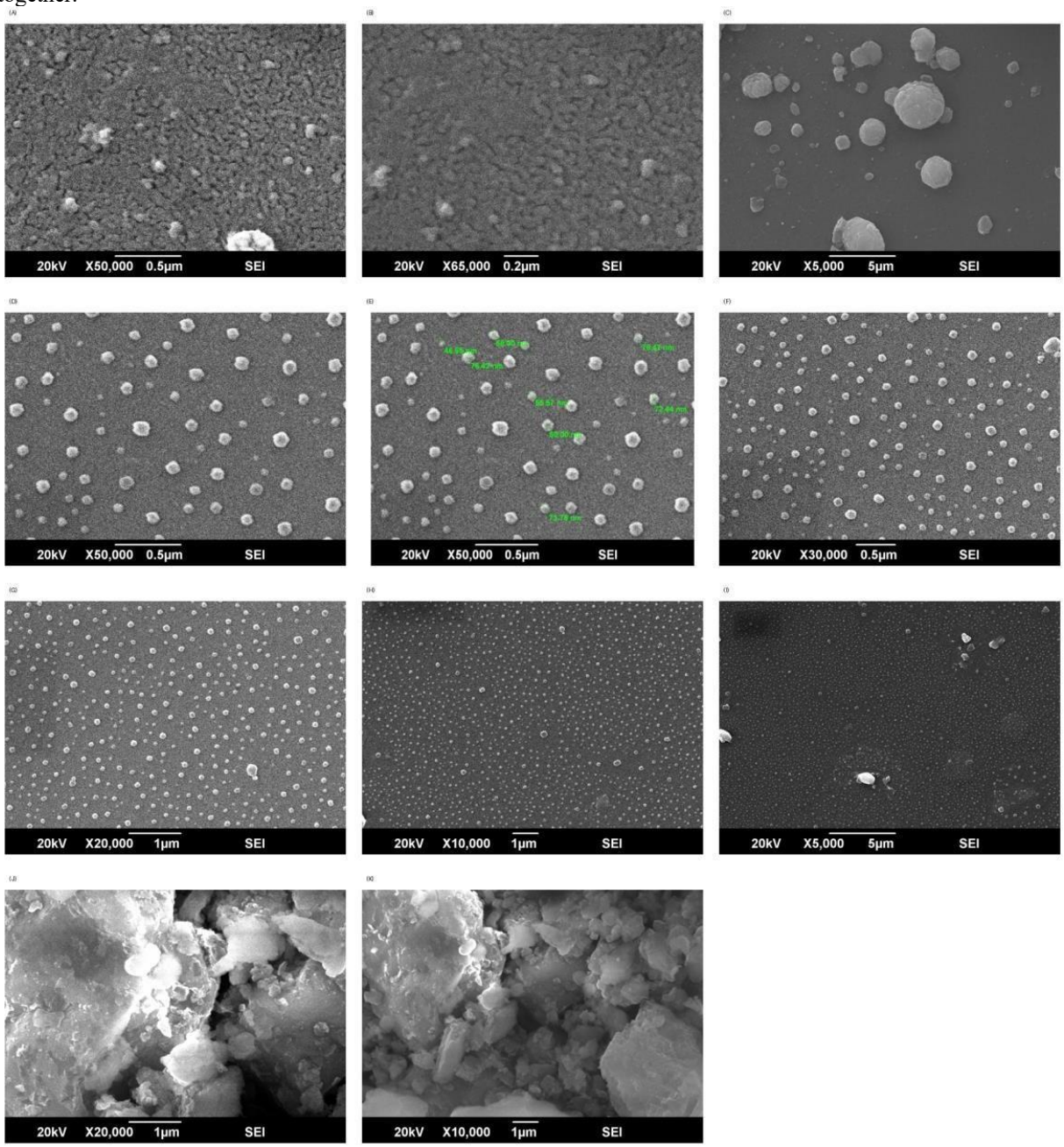

Fig. 4. SEM montage of the synthesized zirconia nanoparticles at multiple magnifications, showing nanoscale primary particles, surface morphology and agglomeration.

3.6. Zeta potential, particle-size distribution and aggregation analysis

The suspension displayed a near-neutral fitted zeta potential of +0.91 mV (raw value +0.42 mV; reported sigma 5.87 mV), indicating minimal electrostatic repulsion. The volume-based particle-size distribution showed a mean diameter of 12.0934 µm, median (D50) of 8.7672 µm, mode of 8.3235 µm and geometric mean of 8.6159 µm. The distribution was broad, with a coefficient of variation of 107.5171% and a span of 1.9714. These values indicate severe aggregation/agglomeration in suspension despite nanoscale primary particles observed by SEM.

Integration of the two size measurements quantified the discrepancy: the volume-weighted mean suspension diameter was approximately 195.1 times larger than the 62-nm SEM mean, while the D50 was approximately 141.4 times larger. This derived comparison highlights colloidal instability as the principal formulation limitation of the unmodified zirconia suspension.

(A) Zeta potential distribution

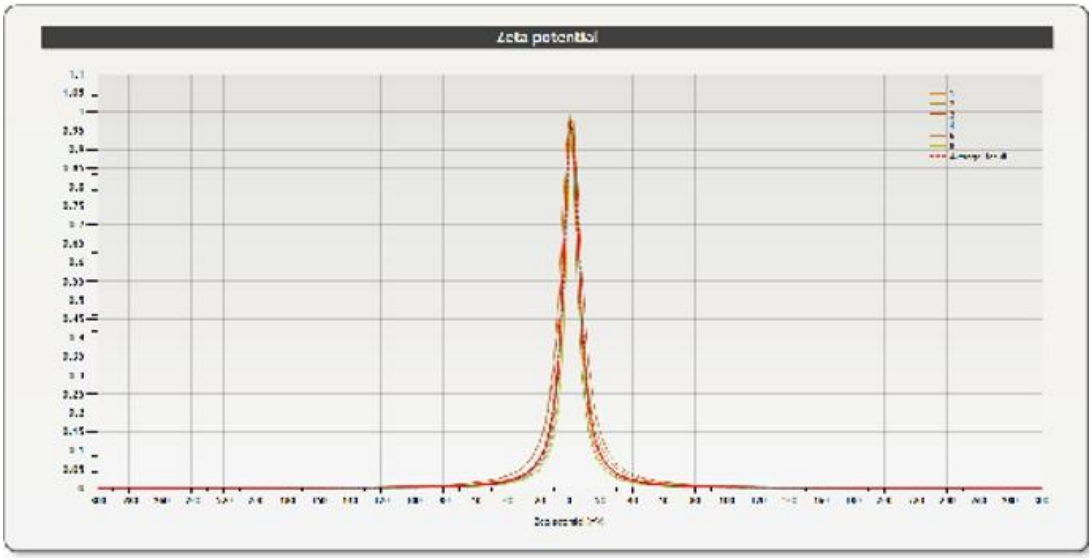

(B) Particle-size distribution graph

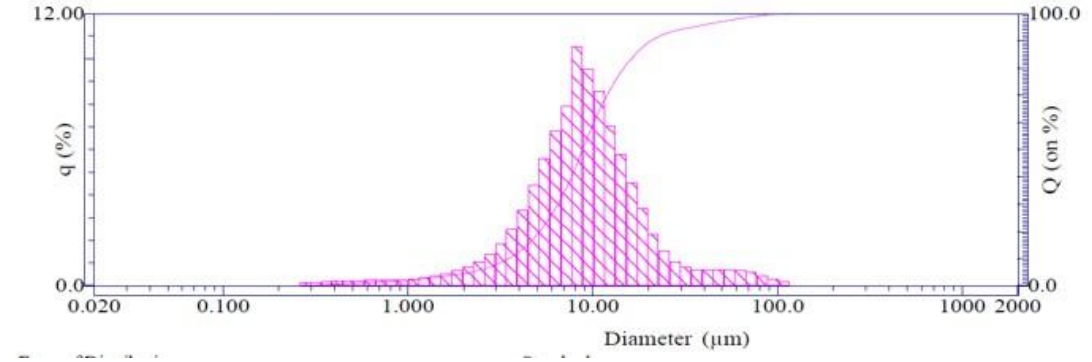

Fig. 5. Zeta-potential distribution and volume-based particle-size distribution of the zirconia nanoparticle suspension. The near-neutral surface charge is consistent with the extensive micron-scale aggregation observed in the PSD.

Table 4. Integrated zirconia nanoparticle characterization and secondary size-analysis summary.

Parameter	Finding
Synthesis appearance	Creamy-white/whitish precipitate or powder
UV-visible	Absorption near 378 nm; reported band-gap ~3.6 eV
FTIR	3425.15, 2920.85, 1629.07, 1433.07 and 1112.53 cm^{-1}
XRD	Crystalline pattern; major reflections ~25-60° 2θ
SEM	Rough/irregular nanoscale particles; mean ~62 nm; agglomeration present
Zeta potential	Fitted mean +0.91 mV; near-neutral surface charge
PSD	Mean 12.0934 µm; D50 8.7672 µm; mode 8.3235 µm; CV 107.5%
Derived size ratio	Mean PSD/SEM ≈195.1; D50/SEM ≈141.4

4. DISCUSSION

The combined results provide a two-stage framework for PCOS-oriented nanotherapeutic development: computational prioritization of a phytocompound and physicochemical evaluation of a candidate inorganic carrier. The 30-ligand docking dataset generated several high-affinity predicted interactions across proteins representing apoptosis, stress response, metabolism, nutrient sensing and protein-quality control. This is compatible with the multi-system biology of PCOS, in which endocrine, metabolic, oxidative and inflammatory pathways interact rather than operate independently [1-5]. Similar In Silico studies have used GC-MS-defined phytochemical libraries to prioritize candidate ligands against PCOS-related protein targets before experimental testing [10,11].

CADIE was retained as the focused lead because of its position in the MAGE-A3 output and its favorable descriptor profile. The -8.00 kcal/mol docking score was not the most negative value in the complete dataset, but lead selection

in this study was based on integrated interpretation rather than docking energy alone. CADIE combined a relatively low molecular weight, modest TPSA, seven rotatable bonds, no Lipinski violation, high predicted gastrointestinal absorption and no predicted P-glycoprotein substrate liability. The 100-ns trajectory further supported persistence of the selected complex, with mean RMSD of 1.4 Å. Nevertheless, MAGE-A3 is not established here as a clinically validated PCOS target. The interaction should therefore be regarded as hypothesis-generating and requires direct biochemical target-engagement experiments before mechanistic claims are made.

The zirconia results similarly require integrated interpretation. The XRD profile supports formation of a crystalline inorganic phase, while SEM demonstrates nanoscale primary particles with a mean size near 62 nm. Plant-assisted metal-oxide synthesis has been used to generate nanoscale materials while reducing reliance on harsh synthetic reagents [12-14]. In PCOS research, multiple nanoparticle platforms have shown the potential to alter endocrine, redox or metabolic outcomes, including selenium- and curcumin-based systems [6-9]. These precedents support the rationale for carrier development but do not establish that any particular nanomaterial will be effective or safe without formulation-specific testing.

The most important material-science finding in the present dataset is the discrepancy between SEM and suspension-based size measurements. A fitted zeta potential of only +0.91 mV places the suspension near electrostatic neutrality, where repulsive forces are weak and aggregation is expected. Consistent with this, the volume-weighted mean diameter was approximately 12.1 μm and the median approximately 8.8 μm. The derived mean aggregate-to-primary-size ratio of about 195 quantifies the extent of clustering. Thus, although nanoscale zirconia particles were successfully produced, the unmodified dispersion should not be described as colloidally stable. Surface modification, pH optimization, ionic-strength control or an appropriate steric stabilizer would be required before reliable drug-loading and delivery studies.

This interpretation strengthens, rather than weakens, the translational value of the study because it identifies a concrete formulation barrier at an early stage. Nanocarriers intended for biological use must be evaluated not only for primary particle dimensions and crystallinity but also for dispersion behavior, since aggregation can alter effective dose, surface area, biodistribution and cellular interaction [13-15]. The present findings therefore support continued development of zirconia as a material platform while showing that colloidal engineering is necessary before biological performance can be predicted.

Future research must directly address the material limitations identified in this study, notably the colloidal instability and aggregation in unmodified zirconia suspensions, by implementing precise colloidal engineering and steric stabilizers

5. CONCLUSION

This study integrated In Silico phytocompound prioritization with zirconia nanoparticle characterization for PCOS-oriented therapeutic development. The 30-ligand docking screen identified multiple high-affinity predicted interactions across the ten-protein panel. CADIE was prioritized in the MAGE-A3 output at -8.00 kcal/mol, showed favorable drug-likeness characteristics, and maintained overall computational stability during a 100-ns molecular-dynamics trajectory. Zirconia synthesis produced a crystalline nanoscale material with an SEM mean size of approximately 62 nm. However, the near-neutral zeta potential (+0.91 mV), micrometer-scale particle-size distribution and ~195-fold aggregate-to-primary-size ratio demonstrate substantial colloidal instability. The combined evidence therefore supports CADIE as a candidate for further experimental validation and zirconia as a structurally promising but formulation-dependent carrier platform. Before therapeutic testing, the zirconia dispersion requires stabilization and the CADIE-MAGE-A3 relationship requires direct biological confirmation.

Ethical Declaration

Not applicable. The present manuscript reports computational analyses and physicochemical nanoparticle characterization and does not present new animal or human experimentation.

Data Availability Statement

The data presented in this manuscript were derived from the finalized PhD research dataset. Underlying tables, docking outputs and nanoparticle characterization records are available from the corresponding author on reasonable request, subject to institutional requirements.

Conflicts of Interest

The author declares no conflict of interest.

REFERENCES

[1] Waqar MA, Mubarak N, Khan R. A comprehensive review on recent advancements in navigating the complexities of polycystic ovarian syndrome (PCOS). Reproductive Sciences. 2026; 33(5): 928-949.

[2] Chen Y, Sun X, Xia X, Chen K, Zeng F. The pathogenesis, therapeutic targets and drugs of polycystic ovary syndrome. Frontiers in Endocrinology. 2026; 16: 1722649.

[3] Siddiqui S, Mateen S, Ahmad R, Moin S. A brief insight into the etiology, genetics, and immunology of polycystic ovarian syndrome (PCOS). Journal of Assisted Reproduction and Genetics. 2022; 39(11): 2439-2473.

[4] Rudnicka E, Duszewska AM, Kucharski M, Tyczynski P, Smolarczyk R. Oxidative stress in polycystic ovary syndrome. Reproduction. 2022; 164(6): F145-F154.
[5] Kisiala M, Mazepa W, Bauer D, Tabaka P, Gas M, Sowinski A, et al. Molecular mechanisms of insulin resistance and altered carbohydrate metabolism in PCOS: A scoping review. Frontiers in Endocrinology. 2026; 17: 1810805.
[6] Shi M, Li X, Xing L, Li Z, Zhou S, Wang Z, et al. Polycystic Ovary Syndrome and the Potential for Nanomaterial-Based Drug Delivery in Therapy of This Disease. Pharmaceutics. 2024; 16(12): 1556.
[7] Butt MA, Tabassum S, Hardy RS, Kiyani MM. Mechanistic insight into nanomedicine for polycystic ovary syndrome. Molecular Biology Reports. 2025; 52(1): 618.
[8] Rabah HM, Mohamed DA, Mariah RA, Abd El-Khalik SR, Khattab HA, AbuoHashish NA, et al. Novel insights into the synergistic effects of selenium nanoparticles and metformin treatment of letrozole-induced polycystic ovarian syndrome: Targeting PI3K/Akt signalling pathway, redox status and mitochondrial dysfunction in ovarian tissue. Redox Report. 2023; 28(1): 2160569.
[9] Raja MA, Maldonado M, Chen J, Zhong Y, Gu J. Development and evaluation of curcumin encapsulated self-assembled nanoparticles as potential remedial treatment for PCOS in a female rat model. International Journal of Nanomedicine. 2021; 16: 6231-6247.
[10] Al-Otaibi WA, AlMotwaa SM. Molecular docking and pharmacokinetic profiling of GC-MS-identified phytochemicals from Peganum harmala-derived essential oil: In Silico assessment of binding affinity toward PCOS-related targets. Applied Sciences. 2026; 16(9): 4214.
[11] Femi-Olabisi JF, Ishola AA, Olujimi FO. Effect of Parquetina nigrescens (Afzel.) leaves on letrozole-induced PCOS in rats: A molecular insight into its phytoconstituents. Applied Biochemistry and Biotechnology. 2023; 195(8): 4744-4774.
[12] Weng G, Li W, Qin F, Dong M, Yue S, Mehmood S, Wang X. Eco-friendly synthesis of zirconia nanoparticles using Sonchus asper extract: A sustainable approach to enhancing Chinese cabbage growth and remediating chromium-contaminated soil. Toxics. 2025; 13(5): 324.
[13] Al Baloushi KSY, Senthilkumar A, Kandhan K, Subramanian R, Kizhakkayil J, Ramachandran T, et al. Green synthesis and characterization of silver nanoparticles using Moringa peregrina and their toxicity on MCF-7 and Caco-2 human cancer cells. International Journal of Nanomedicine. 2024; 19: 3891.
[14] Hosen ME, Rahman MA, Rahman MS, Akash S, Khalekuzzaman M, Alsahli AA, et al. Synthesis of Silver Nanoparticles Using Camellia sinensis Leaf Extract: Promising Particles for the Treatment of Cancer and Diabetes. Chemistry & Biodiversity. 2024; 21(3): e202301661.
[15] Jose A, Mathew M, Aswani R, Parambath Kanoth B, Sebastian KS, Radhakrishnan EK. Zinc oxide nanoparticle mediated modulation of antimicrobial and physico-chemical properties of essential oil containing PVA nanocomposites. Preparative Biochemistry & Biotechnology. 2026; 56(1): 91-110.
[16] Huang X, Zhang S, Liang D, Qiu L, Wu R, Wei R, Chen X, Huang S. BRCA1 alleviates inflammation, oxidative stress, and ovarian granulosa cell apoptosis by inhibiting endoplasmic reticulum stress, thereby ameliorating polycystic ovary syndrome. European Journal of Medical Research. 2026.
[17] Ke Y, Tang D, Yang Q, Zhao H, Zheng J, Zhu C. Anti-Mullerian hormone in PCOS: Molecular regulation and emerging therapeutic strategies. Biomolecules and Biomedicine. 2026; 26(2).
[18] Heshmati J, Moini A, Sepidarkish M, Morvaridzadeh M, Salehi M, Palmowski A, et al. Effects of curcumin supplementation on blood glucose, insulin resistance and androgens in patients with polycystic ovary syndrome: A randomized double-blind placebo-controlled clinical trial. Phytomedicine. 2021; 80: 153395.